Integrated Electric Motor Drive and Power Electronics for Bidirectional Power Flow between the Electric Vehicle and DC or AC Grid

Ch.Mamatha, R.Chander

***Abstract*— This paper presents an integrated traction machine and converter topology that has bidirectional power flow capability between an electric vehicle and the dc or ac supply or grid. The in- ductances of the traction motor windings are used for bidirectional converter operation to transfer power eliminating the need for ex- tra inductors for the charging and vehicle-to-grid converter opera- tions. These operations are in addition to the vehicle traction mode operation. The electric power train system size and weight can be minimized with this approach. The concept has been analyzed with finite-element-coupled simulation with dynamic analysis software. Experimental results are also provided with electric machines. The interleaving technique has been used with the inductors to share the current and reduce the converter switching stresses**

***Index Terms*— Bidirectional converter, electric vehicle, inte- grated converter, machine inductance**

I. INTRODUCTION

The multipurpose use of the power electronic converter in the drive train of an electric vehicle has become an interesting topic for minimizing the system size, weight, and cost. The weight and size of the converter are challenging issues in the case of on-board chargers which otherwise provides the flexibility of charging the vehicle anywhere. The vehicle is not driven during the period of charging, and hence, the traction motor and inverter of the power train can be used as an integral part of the converter. The windings of the traction motor can serve as the inductors of the power converter along with power devices of the traction inverter to transfer power. The power converter of the electric vehicle can draw power from the grid when it requires, and also can deliver power to the grid in the peak time when the grid needs power. During a significant part of the day, most vehicles remain idle in the parking lot when the integrated power converter can use the traction motor and its drive to transfer power to the grid.

Several research activities for integrating the battery charging system with the traction drive have been reported in [1] and [2]. In one approach, the traction motor windings have been used as the inductors for the converter to develop the charging system without any additional component [3]. The three-phase supply is connected with each phase of the machine and the battery is always connected to the dc bus. The research showed the use of a poly-phase machine for the charger. Other topologies have been used for battery charging systems with traction motor windings used as filter components [4]–[6]. An on-board inte- grated charger has been proposed with reconfiguration of the stator windings of a special electric machine in [7]. A battery charger is developed for the electric scooter, where interior permanent magnet traction motor is used for charging with power factor correction [8]. The interleaving technique is another interesting approach used in designing dc–dc converters for reduced switching stresses and increased efficiency [9]–[11]. The approach reduces the size and power rating of the converter passive components. Low EMI and low stress in the switches can be expected from the interleaved converter phase legs [11].

Manuscript received June 13, 2016

In this paper, an integrated motor converter is proposed that can be used as the traction motor drive, a battery charger, and a power converter to transfer energy from vehicle-to-grid (V2G) through reconfiguration of the inverter topology using relays or contactors. The traction inverter with the proposed recon- figuration method can also transfer power from the vehicle to a dc grid and from a dc grid to the vehicle using the traction motor windings with the appropriate relay settings. The three- phase machine windings and the three inverter phase legs can be utilized with an interleaved configuration to distribute the current and reduce the converter switching stresses. The battery voltage is increased in the boost mode to an output reference voltage level within the limits of the machine ratings. A soft starter method using PWM control has been used to reduce the starting current overshot when connecting to a dc grid. In a dc grid connected mode, the voltage drop across the inductor will be the difference between the inverter output voltage and the dc grid voltage. The dc grid voltage provides more stable voltage to counteract the rate of change of inductor current and the current ripple is controlled in a better fashion in a dc grid connected mode.

The proposed converter system can also be used for transfer- ring power between a single-phase ac grid and the vehicle in either direction without any extra component. The rated conditions of the motor and utility interface are quite similar. The inverter is able to regulate the motor phase current in the entire speed range. When changing from the motor control mode to ac grid connected mode of operation, the back EMF voltage is replaced with the grid voltage. Considering the operating conditions with the grid, motor inductance would be enough to handle the grid connected modes of operation. Also, in the blocked rotor condition, motor magnetizing inductance dominates and contributes to the phase inductance significantly. For high enough inductance required in case of ac grid, the rotor can be locked which will give high inductance in the blocked rotor condition. In the charging mode, the machine is thermally stable with no electromechanical power flow through the airgap of the machine. The machine ratings are within limits in all the operating modes as there is only electric loading, and no magnetic loading except during traction operation. The current limit is higher in converter modes compared to the traction mode current limit.

This paper presents the analysis, design, and experiments of the integrated traction drive and power converter for electric/hybrid vehicle applications. The electric machine has been analyzed using coupled simulation of finite-element and dynamic analysis software. The power converter and controller have been modelled using MATLAB/Simulink. The proposed converter reconfiguration method is advantageous for reducing the size and component of the electric power train while providing bidirectional power flow capability with connections to either dc or ac supplies.

II. CONVERTER TOPOLOGY

Different types of topologies have been developed for electric vehicles for battery charging and bidirectional power flow between the battery and the power supply. However, the traction inverter uses the standard six-switch configuration that has elements of the various power converter topologies. The proposed converter topology utilizing the traction inverter along with the switches used for reconfiguration is shown in Fig. 1(a) and (b) shows the detailed switch or relay arrangements required for different modes of operations. Several different configurations can be obtained by appropriate positioning of the switches, which results in a novel methodology for bidirectional power transfer between a vehicle battery and dc or ac grid. Including the use of the topology as the traction inverter during vehicle operation this power converter can be operated in five different modes:

1) power flow from the battery to the dc grid, 2) power flow from the dc grid to the battery, 3) traction mode, 4) power flow from the battery to single-phase ac grid and 5) power flow from a single-phase ac grid to the battery.

The reconfiguration switches can be realized with relays or contactors depending on the ratings of the currents. Those relays and contactors are controlled in a coordinated way to accommodate the different modes of use. The contactors with optimum current capacity should be used to minimize the size of the contactor. The size of the contactor has to be accommodated based on the current rating chosen. To minimize the space and size of the contactors, all the switches can be integrated into a single package.

The switches will be controlled for the different modes of operation using State 1 and State 2 conditions given in Table I. Fig. 1(b) shows the details of the configuration in the routing box with the switches which relates to the operations of the switches according to Table I. The terminal numbers are shown in Fig. 1(b) inside the switches which are changed to different positions for the different configurations. When the converter is to connect to a dc grid, Switch 4 will be in State 1 to isolate from the ac grid.

When the converter is to connect to an ac grid, Switch 5 will be in State 1 to isolate from the dc grid. Thus, the traction converter can be connected to either a dc or an ac grid. Fig. 2 shows the OFF condition where all the switches are in State 1; in this situation, there will be no power transfer. If there is any fault in one or multiple phases in the motor the converter configuration will be switched to State 1 as shown in Fig. 2, and there will be no power transfer between the grid and the battery. The usual protection schemes for a traction inverter will take over. The system has inherent fault protection capability, and extra protection is not needed.

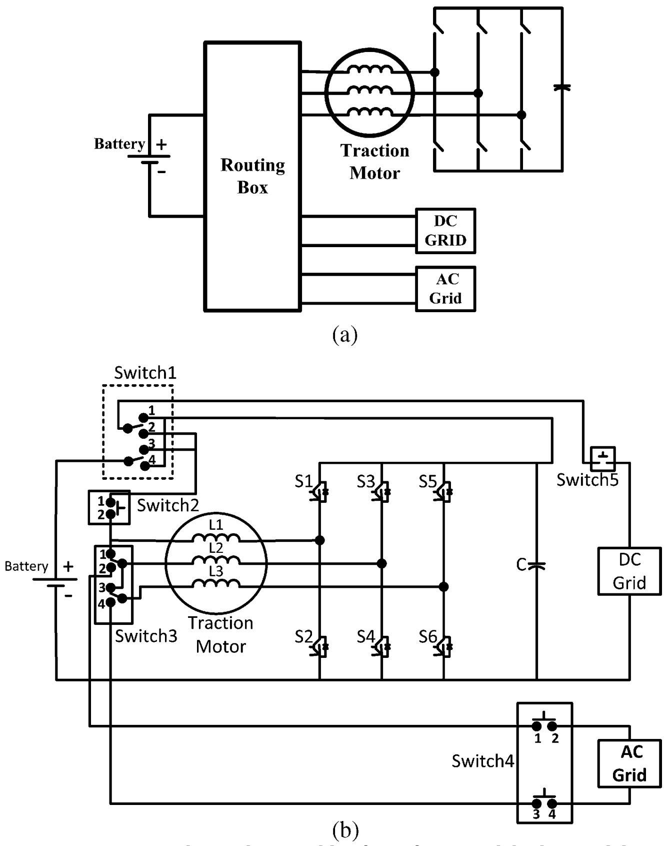

(a) (b)

Fig. 1. Converter with switches capable of interfacing with both ac and dc grid (a) combined and (b) details.

TABLE I SWITCH POSITIONS AND CONVERTER STATES

Switch	State 1	State 2
Switch1	Pole positions:1 and 3	Pole positions: 2 and 4
Switch2	1 and 2 disconnected	1 and 2 connected
Switch3	Pole positions: 1 and 3	Pole positions: 2 and 4
Switch4	1 and 2, and 3 and 4 disconnected	1 and 2, and 3 and 4 connected
Switch5	1 and 2 disconnected	1 and 2 connected

Power is transferred from the vehicle battery to the dc grid using the boost mode of operation for the converter with Switch 2 and Switch 5 in State 2, and the other switches in State 1; power from the vehicle battery to the dc grid can also be transferred in buck mode with Switch 3 and Switch 4 in State 1 and the other switches in State 2. When power transfer is needed from dc grid to the vehicle, Switch 2 and Switch 5 are in State 2 for buck operation and Switch 3 and Switch 4 are in State 1 for boost operation. From Fig. 3, it can be observed that for V2G boost operation, the interleaved technique can be applied on the battery side with the three inductances and three legs of the converter; for G2V boost operation, the interleaved technique can be applied on the dc grid side to reduce the switching stresses.

The proposed converter can be used for traction mode with Switch1 in State 2 and other switches in State 1 as shown in Fig. 5.

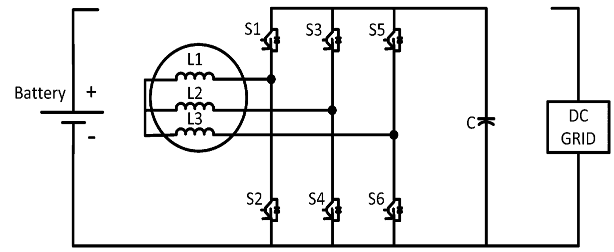

Fig. 2. Circuit with all switches in State

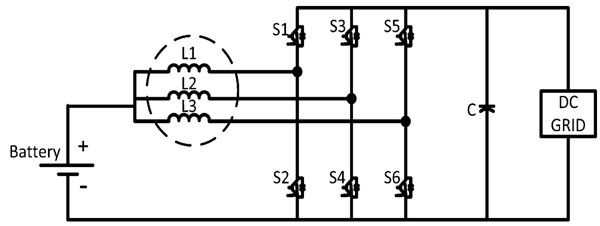

Fig. 3. Circuit with Switch 2 and Switch5 in State 2 for V2G boost or G2V buck operation with vehicle side inductors interleaved.

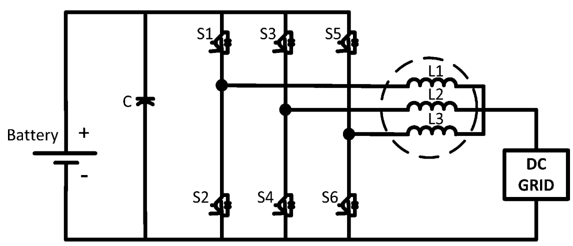

Fig. 4. Circuit with Switch 3 and Switch 4 are in State 1 for V2G buck or G2V boost operation with dc grid side inductors interleaved.

This converter can be used for bidirectional power transfer between a single-phase ac grid and the vehicle battery. For this configuration, Switch 1 and Switch 5 are kept in State 1, while all switches are to be in State 2. The two phases of traction motor windings are connected with the single-phase ac grid side and another switch connects with the battery as shown in Fig. 6. Power can flow in either direction with buck or boost modes of operation.

Operating mode 1 in Fig. 3 and operating mode 2 in Fig. 4 have been verified in simulation. Operating mode 1 is experimentally verified using two types of machines. Although, operating mode 2 in Fig. 4 is different from operating mode 1, the converter is symmetrical for these two modes and for experiments they are similar. Therefore, verifying operating mode 1 experimentally is sufficient for both modes. The operation mode in Fig. 5 is the typical traction machine operation which is used in the motor drives of electric and hybrid vehicles.

The typical traction inverter and its controller are designed to have enough bandwidth to regulate the motor phase currents with reasonable ripple on them. The voltage that appears across the motor inductances is dependent on the inverter dc bus volt- age, amount of motor inductance, motor back EMF voltage, and the switching frequency of the controller. When the inverter switches to the grid connection mode, the effect of back EMF voltage is replaced by the grid voltage and the rest of the elements would stay close to the motor operation. In fact, current regulation during traction at low speed is much more challenging than the grid connected operation since the back EMF voltage is quite small at low speeds. Therefore, the machine inductance would be suitable for all the operating modes, since it is just the configuration of the winding of the machine, and the ma- chine inductances are typically large values. The performance depends on the machine specifications. The maximum current limit is within the thermal limit of the machine, and the ripple in current is dictated by the fixed inductance of the machine as the machine windings cannot be changed. The bus capacitor is selected to handle the voltage ripple and the appropriate switching frequency is selected beyond the acoustic range of frequencies. If there is an option to design the machine with the intention of applying the proposed reconfigurable converters, then the ma- chine can be designed with higher current capability for faster charging and higher winding inductance for minimizing current ripple without degradation of traction operation.

Traction machines can be of induction, permanent magnet, or switched reluctance machine types. Inductance variations for permanent magnet synchronous and induction machines with respect to the position change are minimal. However, there are variations of the inductance value at different rotor positions for interior permanent magnet and switched reluctance machines. With a dc grid, the rotor is not required to be locked as it will be aligned with the maximum inductance path. Consequently, the ripple will be lower. With an ac grid, the flux produced from ac voltage can move the rotor or vibrate the rotor. In this case, the rotor needs to be locked. The mutual inductances have not been modelled in this analysis. There can be phase imbalance due to the mutual inductance. Phase current controls with individual phase current measurements are already in place in a typical traction drive. The current controller would act to compensate for the variations in the inductance and balance the phase currents. The difference in the current ripple between the phases could still be an issue, but is not expected to be a significant one.

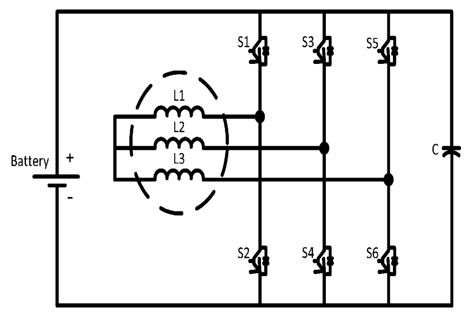

Fig. 5. Circuit with Switch 1 is in State 2 for traction mode operation.

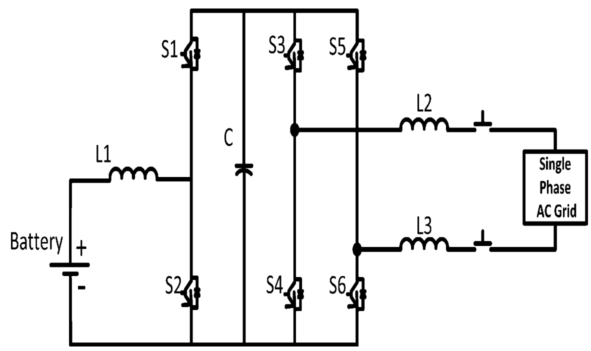

Fig. 6. Circuit configuration for bidirectional interface with a single-phase ac grid.

TABLE II

PARAMETER SPECIFICATION FOR ANALYSIS

Input voltage range	100V – 250V
Maximum output voltage	650V
Machine Phase Inductance	4.98mH
Output Capacitance	3300μF
Load Resistance	20Ω
Maximum Input current	30A

Three-phase machines have been considered in this research as this is the practical scenario with all the traction machines. However, if the phase number is larger than three, three phases will be used and other phases can be distributed and connected to those three branches or the extra phases could be left disconnected depending on the mode of operation. All modes of operation as described in Fig. 3 –Fig. 6 are similarly applicable.

III. SYSTEM ANALYSIS

The converter configuration shown in Fig. 3 can be operated as a simple boost converter if the frequency and duty cycle of the bottom three IGBTs and the top three IGBTs are the same. The system matrix of the converter is

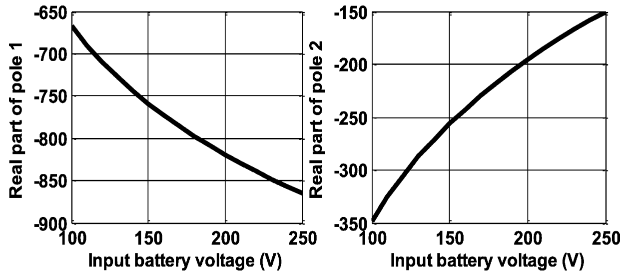

Fig. 7. Effect of input voltage change on the system pole 1 and pole 2.

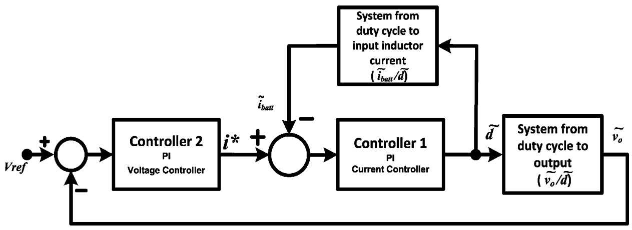

Fig. 8. System block diagram with closed-loop feedback control.

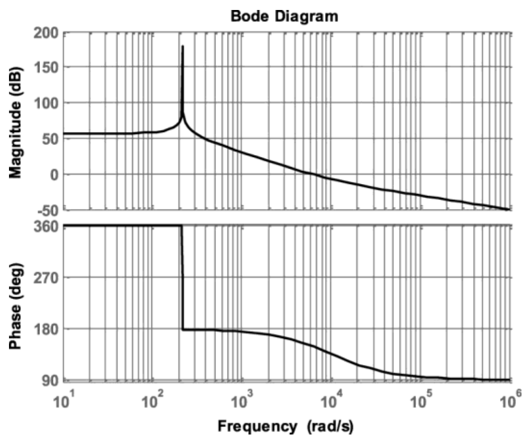

Fig. 9. Frequency response from duty cycle to output voltage.

The transfer functions of duty cycle to output voltage and of duty cycle to battery current can be derived as follows from the small signal analysis of the converter with a PI controller [12] where r_L is the internal resistance of the inductor, D is duty cy- cle, D is $(1 - D)$,L is the combination of the motor windings, and R_L is the combined resistance on the grid side. The system stability can be analyzed using the system matrix.The converter specifications for stability analysis are given in Table II. For the input voltage range of 100–250 V with the desired output voltage of 650 V, the real part of the system poles are observed to be negative (see Fig. 7). The system is stable within these input–output voltage ranges.

The converter characteristics in terms of parameter sensitivity and bandwidth analysis can be analyzed with the closed-loop transfer functions. The corner frequency of the closed-loop sys- tem is

The frequency response of the system for 60% duty cycle with the bandwidth of 6 kHz is shown in Fig. 9. The response would change with change in duty cycle which suggests the parameter dependency of the system transfer function. The converter sys- tem with feedback control as shown in Fig. 8 depends on the duty cycle nonlinearly, which makes it challenging to design this converter within the stability and bandwidth limits [13]. The bode diagram is from the analytical model, which has been used to select the converter parameters.

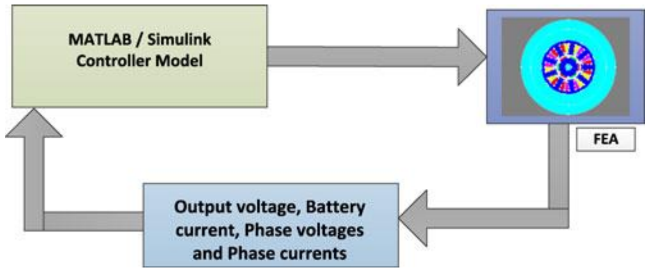

Fig. 10. Coupled simulation of Flux 2-D and MATLAB/Simulink.

IV. SIMULATION RESULTS

In automotive applications, different kinds and ratings of elec- tric machines are used. The applicability of the concept on differ- ent electric machines used in automotive applications is tested with simulation models that would provide the most realistic predictions.

A. Coupled Simulation With MSM

The integrated machine-converter concept has been analyzed through coupled simulation of finite-element and dynamic anal- ysis software where each simulation tool works simultaneously and shares information. An automotive permanent magnet synchronous machine (PMSM) is used. The electric machine modelled in FEA has been integrated with the V2G converter configuration shown in Fig. 3. The machines are modelled in the FEA software Flux2D, while the power converter and controller are modelled in MATLAB/Simulink as given in Fig. 10. The electric machine flux characteristics and the interleaving technique can be analyzed through the coupled simulation with the machine windings sharing the converter current.

The concept has been verified with a small sized three-phase,500 W and surface mount PM machine. The machine has 9 slots and 6 poles. This machine has been integrated with the converter for the same converter topology given in Fig. 3. Fig. 11 shows the connections between the converter and the windings of the machine in finite-element software. The simulation parameters are: battery voltage 12 V, output reference voltage 18 v, and load resistance 0.5 Ω.

Fig. 12 shows that the output voltage settles at the reference voltage of 18 V. The converter currents in the interleaved ma- chine coil windings are shown in Fig. 13; the current ripple is high in these windings since the machine winding inductance is low.

B. Simulation With an Induction Machine

An induction machine is also a common type of electric ma- chine type used in traction applications. A 10 HP, three-phase induction machine where the neutral point is available has been chosen as a traction machine for experimental verification. Dy- namic simulation using MATLAB/Simulink has been done with the inductances of the machine windings. The power transfer characteristics and the interleaving technique for distributing the input currents into the three-phase windings can be ana- lyzed with this simulation.

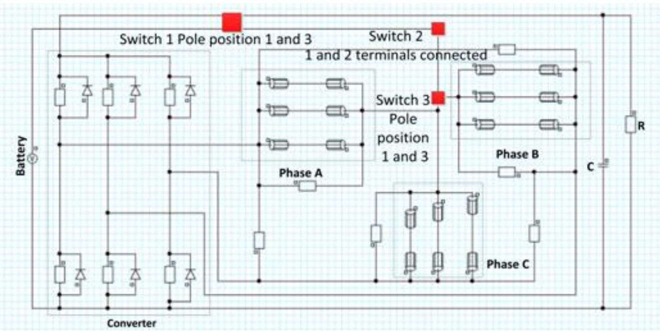

Fig. 11. Converter circuit with motor coil conductors.

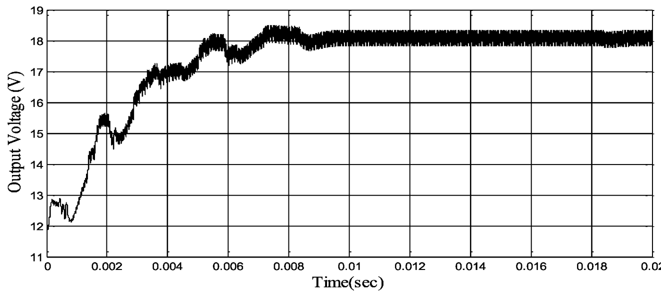

Fig. 12. DC output voltage from coupled simulation.

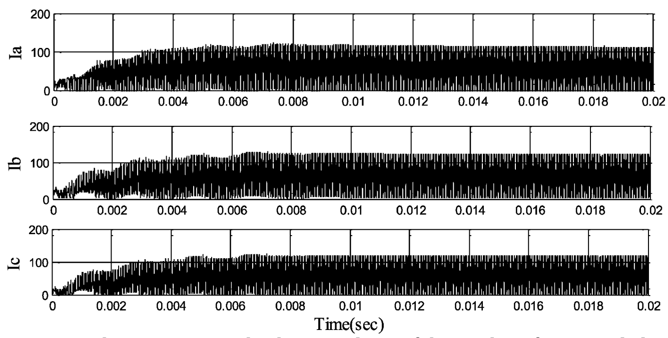

Fig. 13. Phase currents in the three windings of the machine from coupled simulation.

1) Mode 1 and Mode 2 Simulation: Mode 1 is for power flow from the battery to the dc grid and Mode 2 is for power flow from the dc grid to battery. In the simulation, three inductors with the same values of the winding inductance of the induction machine have been used to build the converter as the topology of Fig. 3 for V2G boost mode of operation. The simulation block diagram is shown in Fig. 14(a). The simulation for V2G buck mode of operation using the configuration of Fig. 4 has been

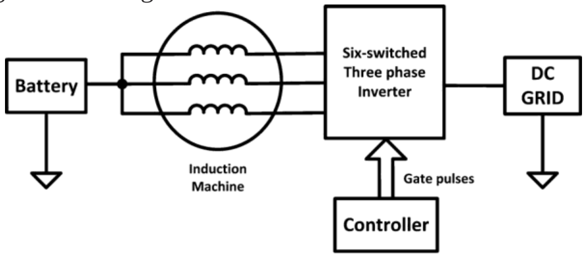

(a)

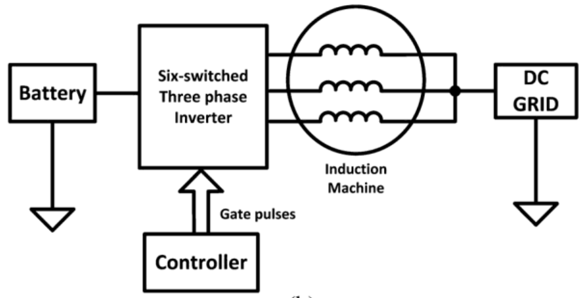

(b)

Fig. 14. Integrated converter and induction machine operation with dc grid; (a) V2G boost mode of operation and (b) V2G buck mode of operation.

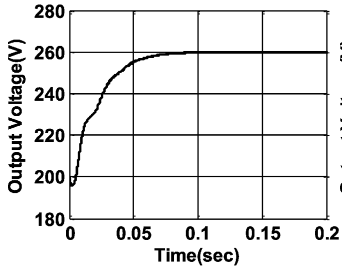

(a)

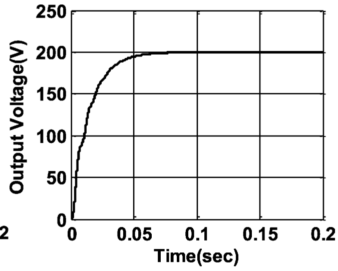

(b)

Fig. 15. Output voltage in Mode 1 and Mode 2 of the integrated mo- tor/converter: (a) for boost operation, and (b) for buck operation.

also done; the simulation block diagram for this mode is shown in Fig. 14(b).

The simulation parameters for boost operation are: input volt- age is 200 V, output reference voltage is 260 V, maximum input current limit is 30 A, induction machine phase inductance is
5 mH, output capacitor is 3300 μF, load resistance is 20 Ω, and PWM switching frequency is 20 kHz. From the simulation re- sult shown in Fig. 15(a), it is observed that the output voltage is following the reference voltage of 260 V in the boost mode of Fig. 3. The simulation parameters for buck operation are: input voltage is 400 V, output reference voltage is 200 V, maximum input current limit is 30 A, induction machine phase inductance is 5 mH, load resistance is 10 Ω, and PWM switching frequency is 20 kHz. From the simulation result shown in Fig. 15(b), it is observed that the output voltage is following the reference voltage of 200 V in the buck mode of Fig. 4.

In the case of boost operation, the output power level is 4 kW. The interleaving technique has been applied in the battery side of the system as shown in Fig. 3 and Fig. 14(a).

The results in Fig. 16 show that the input current can be equally shared through the windings of the three-phase induction machine.

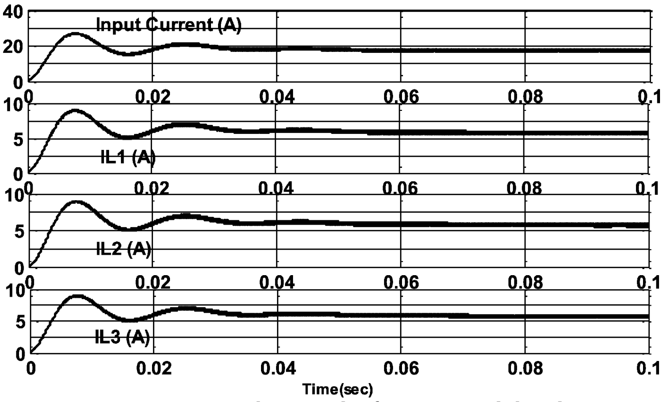

Fig. 16. Input current in boost mode of operation and shared input currents in the three-phase windings on the machine.

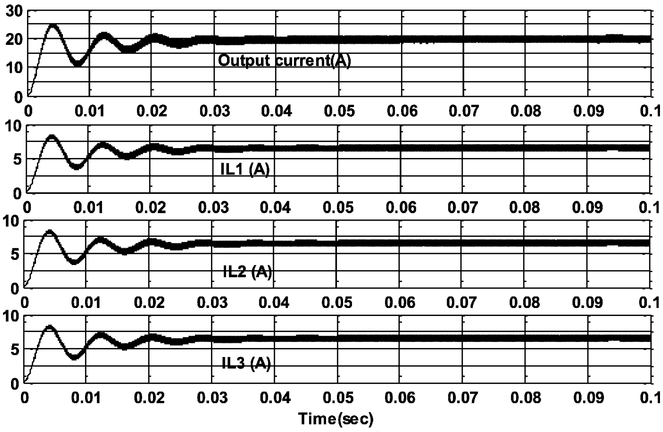

Fig. 17. Output current in buck mode of operation and shared output currents in the three-phase windings on the machine.

In the case of buck operation, the interleaving technique has been applied in load side of the system shown in Fig. 4 and Fig. 14(b). The results in Fig. 17 show that the output current can be equally shared through the windings of the three-phase induction machine.

2) Mode 4 and Mode 5 Simulation: Mode 4 and Mode 5 allow power flow from the battery to a single phase ac grid and from a single phase ac grid to battery, respectively. In the simulation, three inductors of the same values as that of the induction machine have been used in the topology of Fig. 6. The simulation models for Mode 4 and Mode 5 are given in Fig. 18(a) and (b).

For power transfer between the battery and an ac grid, the converter is configured in two stages with a dc/dc converter using one phase leg followed by an H-bridge inverter that interfaces with the ac grid (see Fig. 6). A single phase PLL algorithm has been developed to synchronize the inverter with the single- phase grid. In the PLL algorithm, the grid voltage is first shifted by 90° and then dq-transformation on the grid and the shifted voltages gives the d-axis and q-axis voltages. To lock the phase, the q-axis voltage has been kept at zero by using a loop filter.

The converter is operated in the current controlled mode when interfaced with the grid. Current regulation in the dq domain has been used in the grid connected mode using grid current

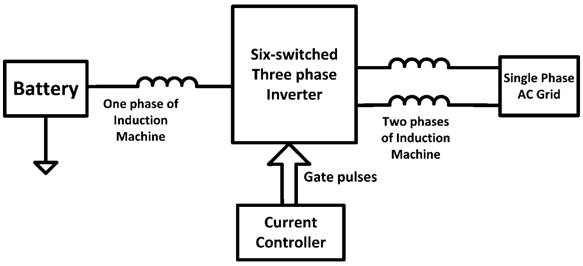

(a)

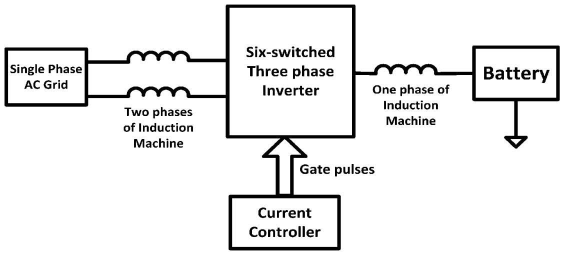

(b)

Fig. 18. Power flow between the battery and an ac grid: (a) from battery to ac grid (Mode 4), and (b) from ac grid to battery (Mode 5).

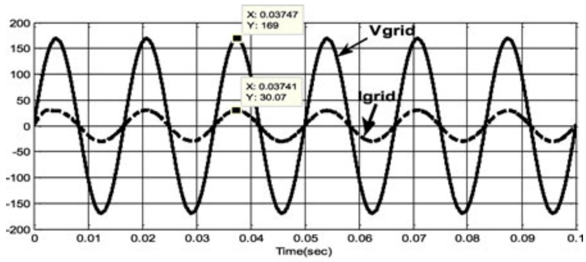

(a)

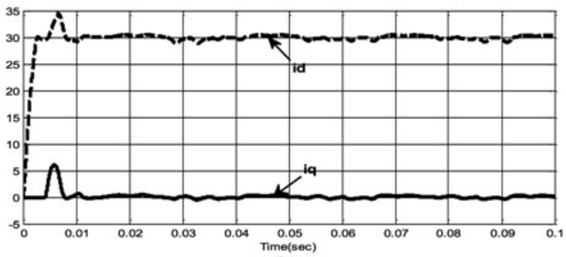

(b)

Fig. 19. Voltages and currents in Mode 4: (a) grid voltage and grid current, and (b) command i_d and i_q currents.

feedback converted to dq current [14]. The amount of power transferred from grid to vehicle and V2G depend on the i_d and i_q current commands. The current regulator design is based on the following dynamic equations:

$$v_d(t) = Ri_d(t) + L\frac{di_d}{dt} - \omega L i_q(t) + e_d(t)$$

$$v_q(t) = Ri_q(t) + L\frac{di_q}{dt} - \omega L i_d(t) + e_q(t)\,.$$

Fig. 19(a) and (b) shows the grid voltage and grid current in Mode 4 with a current command i_d of 30 A and i_q of zero. In this case, the power is being transferred from the vehicle to the single-phase ac grid. The power transferred and the grid currents for different current commands i_d are given in Table III.

TABLE III
POWER FLOW AT DIFFERENT LEVELS IN MODE

4

id (A) Command	Vgrid (RMS) (V)	Igrid (RMS) (A)	Active Power (W)
10	120	7.19	863
15	120	10.52	1262
20	120	14.36	1723
25	120	17.82	2138
30	120	21.17	2540

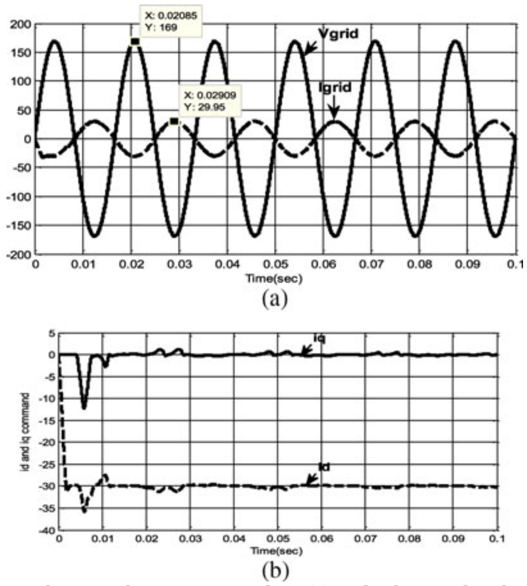

Fig. 20. Voltages and currents in Mode 5: (a) grid voltage and grid current, and (b) command i_d and i_q currents.

TABLE IV
POWER FLOW AT DIFFERENT LEVELS IN MODE 5

id (A) Command	Vgrid (RMS) (V)	Igrid (RMS) (A)	Active Power (W)
-10	120	7.14	857
-15	120	10.6	1272
-20	120	14.29	1715
-25	120	17.68	2122
-30	120	21.29	2555

Fig. 20(a) and (b) shows the grid voltage and grid current in Mode 5; in this case, the current command i_d is –30 A and i_q is zero. Power is being transferred from the single-phase ac grid to the vehicle. The power transferred to the battery and the grid currents for different current commands i_d are given in s Table IV.

V. EXPERIMENTAL RESULTS

The integrated machine-converter concept has been investi- gated with a three-phase inverter and machine inductors. The converter has been tested in the boost configuration of Fig. 3 which represents the vehicle to dc grid power transfer mode.

A standard three-phase, six-switch IGBT inverter module is used as shown in Fig. 21(a). The voltage rating of the inverter is 1200 V and the current rating is 100 A. The dc bus capacitor is 3300 μF. A system controller has been built around a microchip dSPIC33 digital signal processor. The controller board as Fig. 21(b) has been built with the processor, sensors, analog signal conditioning, and several fault protection circuitry.

Fig. 21. Experimental Setup: (a) three-phase IGBT module, and (b) controller board.

TABLE V RESULTS
WITH PMSM

Input Voltage (V)	Input current (A)	Output Voltage (V)	Output current (A)	Output Power (W)	Efficiency
11.8	10.9	17.5	6	105	81.64%
11.5	36.5	18.7	19.3	360.91	85.98%
10.8	53.5	21.9	22.2	486.18	84.14%
10.4	61.1	22.8	23	524.40	82.53%

Fig. 22. Experimental setup with PMSM.

A. *Experiment With PMSM*

The power transfer from voltage source to load was successfully done using the machine phase inductances. The PM machine available with neutral connection and chosen for experimental verification is a 500 W, 12 V, 9/6 (slots/poles) PMSM as given in Fig. 22. The phase resistance and phase inductance of the machine are 10.25 mΩ and 35 μH, respectively. This is the same PMSM used in the FE analysis. The machine was disassembled to gain access to the neutral point for conducting experiments in this project.

The phase windings were used in the interleaved boost converter configuration of Fig. 3 for transferring power from the battery to the load using the machine inductance. Experiments were conducted up to the rated 500 W of the PMSM and the results are presented in Table V. Voltages and currents captured by the oscilloscope for about 100 W power transfer with voltage boosted from 12 to 18V are shown in Fig. 23.

The current ripple seen in Fig. 23 is higher than expected since the 9/6 PMSM used for experimental verification of the proposed converter with reconfiguration is a lower power ma- chine with low inductances. Fig. 13 also showed the high current ripple, since the same machine is used in the simulation. This machine is used only for verifying the concept. A typical traction machine power level is much higher and the inductance is also higher than that used in simulation and experiments. Therefore, the current ripple with a practical traction machine will be much less than the presented simulation and experimental results in Figs. 13 and 23. The result with the higher power-rated induction machine showed that the current ripples are indeed much smaller. The efficiency results with the PMSM are also inherently low since this is a low power, low-voltage machine designed for torque ripple sensitive applications where efficiency is not the critical design parameter. As it is shown later, the efficiency results with the higher power-rated induction machine that was designed for efficiency sensitive applications has a comparatively higher efficiency; also, the efficiency trends with load is also more meaningful with this machine.

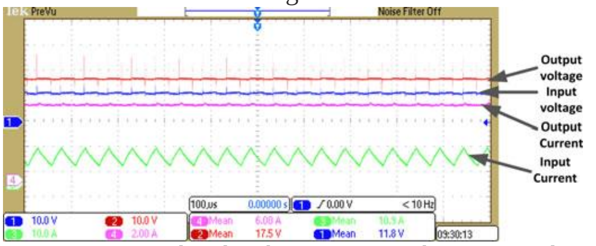

Fig. 23. Experimental result with PMSM: input voltage, output voltage, input and output currents.

As long as the voltage and current ratings of the machine are maintained during power transfer, the machine inductance behaves similar to a standalone inductor. Resistive loads are used as the output for simulating the dc grid, but the dc bus voltage is regulated to keep it close to the level of battery voltage. The dc bus voltage, which refers to the output voltage, can be changed with given reference voltages and with different loads. In this experiment with the 12 V PMSM, the voltage level was kept close to the battery voltage. The voltage level can be set to the desired output voltage level. By setting the reference value of the output voltage the battery can be charged safely. Depending on the battery pack state of charge and the battery chemistry, the reference value of the battery charging voltage can be set to dictate the charging rate. As the battery's state of charge increases, the current that is drawn from the charger reduces.

The resistive load does not exactly represent the characteristics of a dc grid since there could be nonlinear effects from the batteries or other loads. The effects of these nonlinearities could be dealt with better control techniques during dc grid operation, but the proof of concept is still valid with resistive load testing. With an ac grid, the inverter can supply to a reactive load [8].

B. Experiment With an Induction Machine

A 10HP three-phase induction machine has been used to integrate the converter to transfer power from the dc supply to resistive load. The windings of the induction machine are configured for the low voltage range of 208 –230 V. The current rating of the machine is 25 A, the rated speed is 1755 rpm, and the phase inductance is 4.98 mH. The motor windings are reconfigured by changing the pole position of the switches.

TABLE VI
EXPERIMENT PARAMETER SPECIFICATION

Input battery voltage	200V–400V
Input current	30A
DC bus voltage	200V–650V
Output current	30A
Power	15kW
Output capacitor	3300μF
Load resistance	20Ω
Switching frequency	20 kHz

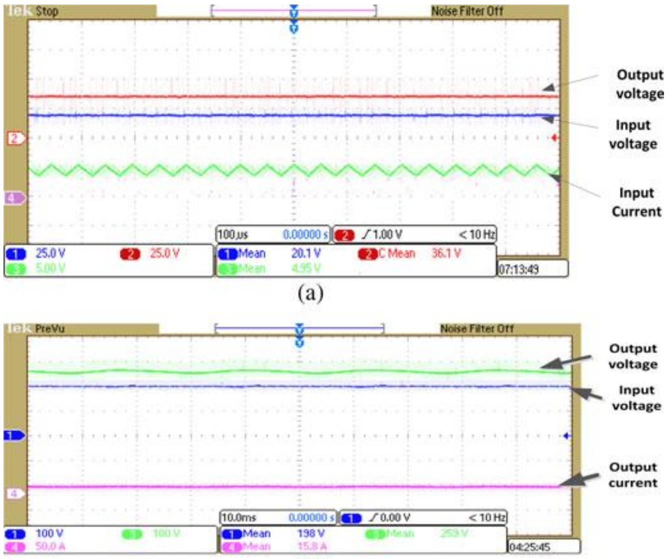

(a) (b)

Fig. 24. Experimental result with Induction Machine: (a) input voltage and current and output voltage in low power level, and (b) input voltage and current and output voltage in high power level.

The interleaving technique with the three-phase windings of the induction machine is first tested. The three winding inductances have been interleaved in the battery side of the converter. The controller is set to boost the voltage from the battery side to dc grid side for V2G operation with the configuration of Fig. 3. A 400 V and 25 A rating dc supply is used as an input. A re- sistive load is used on the dc output side. The experiments have been done up to 4 kW level.

The converter designed can work up to 70% duty cycle within the input–output voltage range for the specifications given in Table VI for boost operation. In the case of buck operation, it can work up to 50% duty cycle. The conventional bidirectional converter used in traction power train configurations can handle only one way boost and one way buck, but this converter can handle buck and boost operation in either way with overlapping input and output voltage ranges. The control loop regulates the output voltage.
Fig. 24(a) shows the experimental result for low power level with input current shown for one phase of the induction machine winding. The input and output voltages shown in Fig. 24(b) for a power transfer level of 4 kW; the input and output voltages are 198 and 259 V, respectively. The current ripples in the figure include high frequency measurement noise in addition to the switching ripple. The switching ripple is only up to 2 A since the machine inductance is high. The current ripple magnitude depends on the inductance value of the traction motor.

TABLE VII
RESULTS WITH INDUCTION MACHINE

Input voltage (Vin)	Input current (A)	Input Power (W)	Output Voltage (Vo)	Output Current (A)	Output Power (W)	Efficiency (%)
148	14.2	2101.6	193	9.53	1839.29	87.52%
196	10.6	2077.6	260	7.12	1851.2	89.10%
195	16.5	3217.5	236	12.2	2879.2	89.49%
198	22.9	4534.2	259	15.8	4092.2	90.25%

The experimental result provided in Fig. 24(b) matches with the simulation result. In the simulation, the output voltage goes to 260 V and output power is 4 kW and in the experiment, the same output voltage and power have been found for the same topology of Fig. 3. The input current sharing is similar in the experiment as that in the simulation. For a traction machine, the phases are balanced and the current sharing is achieved through implementing the current regulation. The compensation for differences in the phase inductances is managed by the controller since the phase currents are regulated individually. Phase cur- rent equalization system could be considered [8] if the variation in the inductance is significant and the individual current regulation mechanism is not available in the controller.

The input/output power analysis with efficiency calculations for the V2G operation is given in Table VII. The efficiency is low for low voltage and power levels but improves with higher input/output voltages and power levels as expected. Table VII shows the experimental results with different reference output voltages and different power levels. The load values were changed in the experiment to adjust with the power level and different reference output voltages.

In the experiment with the induction machine, the output voltage refers to the dc link or bus voltage. The dc-link voltage can be fixed or variable; it depends on the application. Most of the time dc-link voltage is connected to the dc grid and the dc grid voltage is either collectively or individually controlled by the units that are connected to the grid. For master/slave configuration, typically the strongest unit connected to the grid works in voltage controlled mode and other slave units work in power controlled mode. The dc-link voltage is assumed variable for the experimental results given in Table VII, but the values are within the limits of the specified dc grid operation. In the experiment, the system was controlled in output voltage control mode, where the different reference voltages were set by the controller. The input/output voltage ratio was varied to collect the experimental data at different input voltage levels.

The power transfer between the battery and the ac grid for Mode 4 and Mode 5 of the integrated motor/converter reconfigurability concept has also been verified experimentally using inductors of the same values as that of the induction machine. Fig. 25 shows the experimental result for Mode 4 where the battery voltage is 200 V, the ac grid voltage is 120 V (RMS), and the *dq* current commands are i_d = 30 A, and i_q = 0 A, respectively.

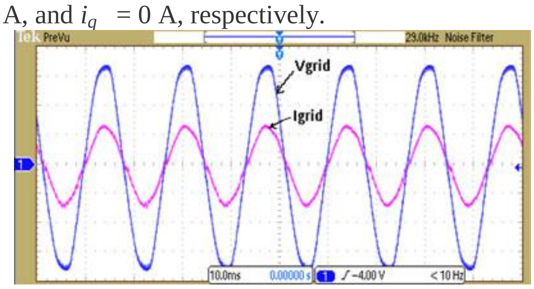

Fig. 25. Experimental result of V_{grid} and I_{grid} for Mode 4 (power flow from battery to a single-phase ac grid).

CONCLUSION

An integrated machine-converter topology and reconfiguration method have been proposed in this paper, where traction machine windings can be used as the inductors of the converter to transfer power between a vehicle battery and either a dc or an ac grid. The converter reconfiguration concept is useful in minimizing the size and parts in the power train of an electric vehicle. The machine-converter coupled simulation results showed that the integrated converter can be used for the power transfer with versatility without significantly extra power elements. The converter performance can be analyzed with the coupled simulation of FEA software and a dynamic simulation tool. The experimental results verified that the proposed inte- grated converter can work in both directions for V2G and G2V; additionally, it has the advantages of utilizing the interleaving technique in both V2G and G2V modes of operations.

REFERENCES

1. S. Lacroix, E. Laboure, and M. Hilairet, "An integrated fast battery charger for electric vehicle," in Proc. IEEE Veh. Power and Propulsion Conf., Oct.2010, pp. 1–6.
2. M. Milanovic, A. Roskaric, and M. Auda, "Battery charger based on double-buck and boost converter," in Proc. IEEE Int. Symp. Ind. Electron., Jul. 1999, vol. 2, pp. 747–752.
3. A. G. Cocconi, "Combined motor drive and battery recharge system," U.S.Patent 5 341 075, 23 Aug. 1994.
4. S. K. Sul and S. J. Lee, "An integral battery charger for four-wheel drive electric vehicle," IEEE Trans. Ind. Appl., vol. 31, no. 5, pp. 1096–1099, Sep./Oct. 1995.
5. D. Thimmesch, "An SCR inverter with an integral battery charger for electric vehicles," IEEE Trans. Ind. Appl., vol. IA-21, no. 4, pp. 1023–1029, Jul./Aug. 1985.
6. L. Solero, "Nonconventional on-board charger for electric vehicle propul- sion batteries," IEEE Trans. Veh. Technol., vol. 50, no. 1, pp. 144–149, Jan. 2001.
7. S. Haghbin, S. Lundmark, M. Alaku¨ la, and O. Carlson, "An isolated high power integrated charger in electrified vehicle applications," IEEE Trans. Veh. Technol., vol. 60, no. 9, pp. 4115–4126, Nov. 2011.
8. G. Pellegrino, E. Armando, and P. Guglielmi, "An integral battery chargerwith Power Factor Correction for electric scooter," in Proc. IEEE ElectricMach. Drives Conf., May 2009, pp. 661–668.
9. N. M. L. Tan, T. Abe, and H. Akagi, "A 6-kW, 2-kWh Lithium-Ion battery energy storage system using a bidirectional isolated DC-DC converter," in Proc. Power Electron. Conf., Jun. 2010, pp. 46–52.
10. S. Dwari and L. Parsa, "An efficient high-step-up interleaved DC–DCconverter with a common active clamp," IEEE Trans. Power Electron., vol. 26, no. 1, pp. 66–78, Jan. 2011.
11. O. Hegazy, J. Van Mierlo, and P. Lataire, "Analysis, modeling, and im- plementation of a multidevice interleaved DC/DC converter for fuel cell hybrid electric vehicles," J. Power Electron., vol. 27, pp. 4445–4458, Jul.2011.
12. O. Hegazy, J. Van Mierlo, and P. Lataire, "Control and analysis of an integrated bidirectional DC/AC and DC/DC converters for plug-in hybrid electric vehicle applications," J. Power Electron., vol. 11, no. 4, pp. 408–417, Jul. 2011.
13. O. Ellabban, O. Hegazy, J. Van Mierlo, and P. Lataire, "Dual loop digi- tal control design and implementation of a dsp based high power boost converter in fuel cell electric vehicle," in Proc. IEEE Int. Conf. Optim. . Electr. Electro. Equipment, May 2010, pp. 610–617.
14. M. N. Arafat, S. Palle, Y. Sozer, and I. Husain, "Transition control strategy between standalone and grid-connected operations of voltage-source in-verters," IEEE Trans. Ind. Appl., vol. 48, no. 5, pp. 1516–1525, Sep./Oct.2012.